THE ARCHIVES OF TRANSPORT

VOL. XXII NO 2 2010

10.2478/v10174-010-0012-3

Ride comfort for various passenger positions in a railway vehicle – simulation study

Ewa Kardas-Cinal*

Received January 2010

Abstract

The paper presents the analysis of ride comfort of a railway vehicle based on the results of numerical simulations for a model of a passenger car moving along a tangent track with random geometric irregularities. The lateral and vertical rms accelerations in 1/3 octave frequency bands as well as the weighted rms accelerations are calculated at several positions within the car body for two track sections with different track condition and for various vehicle velocities. The obtained accelerations are compared with the comfort and decreased fatigue boundaries according to the ISO 2631-1 and PN-91/S-04100 standards.

Keywords: railway vehicle, ride comfort, passenger position, track condition

1. Introduction

Ride comfort in railway vehicles is determined by various adverse conditions to which passengers are exposed [1,12] during travel. These conditions include, among many others, noise, air humidity, lighting conditions and passenger seat quality as well as their duration which is also an essential element. The present work deals only with the analysis of vehicle vibrations which are usually considered to be the main factor determining ride comfort [2,3,10]. This analysis is based on numerical simulations of vehicle motion and it is focused on vehicle body accelerations, both lateral and vertical, calculated at various positions inside the passenger car for track sections with different track condition. The simulation results for the rms values of these accelerations in 1/3 octave frequency bands are compared with the comfort and decreased fatigue boundaries according to the ISO 2631-1 standard [4] and the

* Warsaw University of Technology, Faculty of Transport, 75 Koszykowa St., 00-662 Warsaw, Poland, e-mail: ekc@it.pw.edu.pl

Polish PN-91/S-04100 standard [11]. The weighted values of these rms accelerations are also compared with the corresponding limits, included in the above standards. This work is continuation of the author's previous works on the ride comfort [6,8,9].

2. Ride comfort – spectral analysis

2.1. Calculation method – rms accelerations

The ride comfort due to vibrations depends on the magnitude acceleration experienced by a travelling passenger, its direction and frequency content. In this work, lateral and vertical components $a_{yb}(t)$, $a_{zb}(t)$ of the vehicle body acceleration obtained in simulations are used to evaluate the vibration-related comfort, following the ISO 2631-1 [4] and standard PN-91/S-04100 [11] standards. The ride comfort evaluation is done by calculating – from the simulation results – the rms acceleration values $a_{yb;\mathrm{rms}}(f_k)$, $a_{zb;\mathrm{rms}}(f_k)$ for the centre frequencies f_k of the 1/3 octave bands $(f_k-\Delta f_k/2, f_k+\Delta f_k/2)$ of width $\Delta f_k = 0.231 f_k$ which are given in the aforementioned standards. This is followed by comparing the obtained rms accelerations with the reduced comfort and fatigue-decreased proficiency boundaries. It should be noted here that these boundaries, shown in Fig. 1, depend on the frequency in such a way that the most sensitive frequency ranges are 4-8 Hz for the vertical direction of acceleration and below 2 Hz for the lateral one which is related to different sensibility of various organs in human body to vibrations from different frequency ranges.

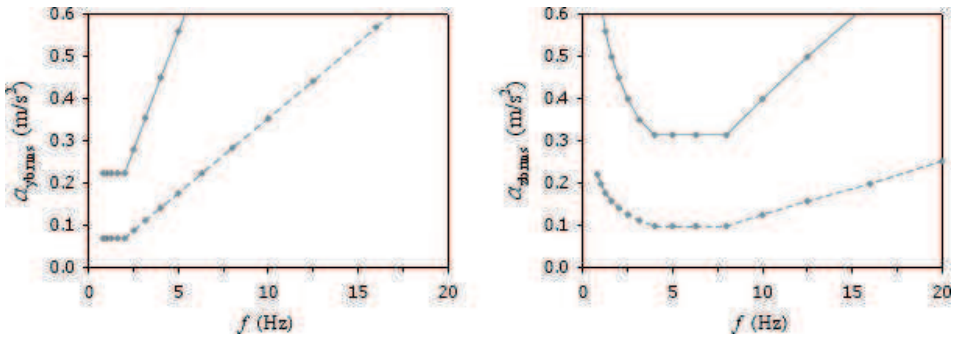

Fig. 1. The reduced comfort (dashed line) and fatigue-decreased proficiency (solid line) boundaries for lateral and vertical rms body acceleration (left panel) and (right panel) and duration for 8 hours [4,11]

The rms value of body acceleration in the k-th band 1/3 octave band is obtained by integrating the power spectral density (PSD) over the corresponding frequency interval:

$$a_{\eta b;\mathrm{rms}}(f_k) = \left(\int_{f_k-\Delta f/2}^{f_k+\Delta f/2} S_{\eta b}(f)\, df \right)^{1/2} \quad (\eta = y, z)\,. \tag{1}$$

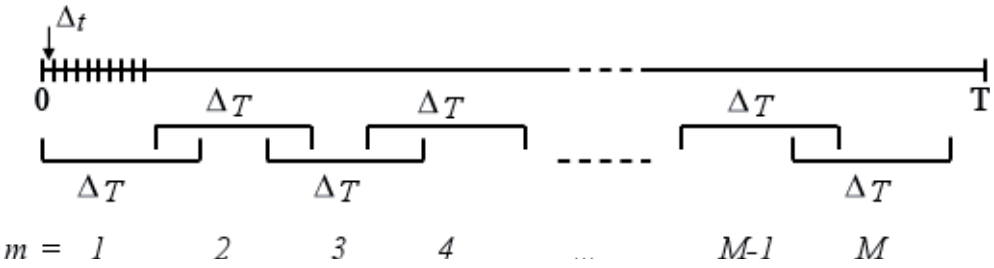

Fig. 2. Schematic arrangement of the time subintervals $\left(T_{\mathrm{o}}^{(m)}, T_{\mathrm{k}}^{(m)}\right)$ used in the Welch modified periodogram method

The PSD $S_{\eta b}(f)$ of lateral ($\eta = y$) and vertical ($\eta = z$) accelerations is calculated with the Welch modified periodogram method [14] on the basis of the acceleration values $a_{\eta b}(t)$ obtained (at equidistant times $t = t_i = i\Delta t, i = 0, 1, 2, \ldots, N$) by numerical simulation of the vehicle motion over the time interval $(0, T)$. The modified periodogram method uses a set of M overlapping time subintervals $\left(T_{\mathrm{o}}^{(m)}, T_{\mathrm{k}}^{(m)}\right)$ (such that $T_{\mathrm{o}}^{(m+1)} < T_{\mathrm{k}}^{(m)}$, $T_{\mathrm{o}}^{(0)} = 0$, $T_{\mathrm{k}}^{(M)} \approx T$), each of which has the same length $T_{\mathrm{k}}^{(m)} - T_{\mathrm{o}}^{(k)} = \Delta T$ several times smaller than the total duration of the vehicle motion T; see Fig. 2 Then, for each time subinterval the original periodogram formula is applied to find – for given frequency f – the quantity

$$S_{\eta b}^{(m)}(f) = \frac{2}{\Delta T} \left| \int_{T_{\mathrm{o}}^{(m)}}^{T_{\mathrm{k}}^{(m)}} a_{\eta b}(t)\, e^{i2\pi f t} dt \right|^2 \tag{2}$$

and the final PSD is calculated as the arithmetic average

$$S_{\eta b}(f) = \frac{1}{M} \sum_{m=1}^{M} S_{\eta b}^{(m)}(f)\,. \tag{3}$$

2.2. Results – evaluation of ride comfort with rms accelerations

The motion of a passenger car is simulated using a non-linear model of a railway vehicle with 27 degrees of freedom and linear characteristics of primary and secondary suspensions [6,13]. The model parameters, including stiffness constants and damping coefficients as well as masses and inertia moments of the car body,

bogies and wheelsets are the same as previously used in [6,13]. The non-linear wheel (UIC 60) and rail (ORE S1002) profiles are used and the forces at the wheel/rail contact are calculated with Kalker's simplified nonlinear theory [5]. The vehicle moves with constant velocity v along a stiff, tangent track with geometrical irregularities: lateral and vertical deviations $y_w(x), z_w(x)$ of the track centre line, variable track gauge $2l$ and local superelevation $h_w(x)$ here x denotes the position along the track. Simulations for various velocities are done for two track sections (I and II) of different track quality (QN1, QN2, respectively) determined by magnitude of track geometrical irregularities. The standard deviations of $y_w(x), z_w(x)$, $2l$ and $h_w(x)$ are 0.00078 m, 0.00090 m, 0.00119 m, 0.00095 m for track section I and 0.00080 m, 0.00128 m, 0.00198 m, 0.00199 for track section II. The PSD functions found for the lateral and vertical track irregularities have significantly different dependences on spatial frequency f_s (= f/v) for track section I than for track section II; see Fig. 3.

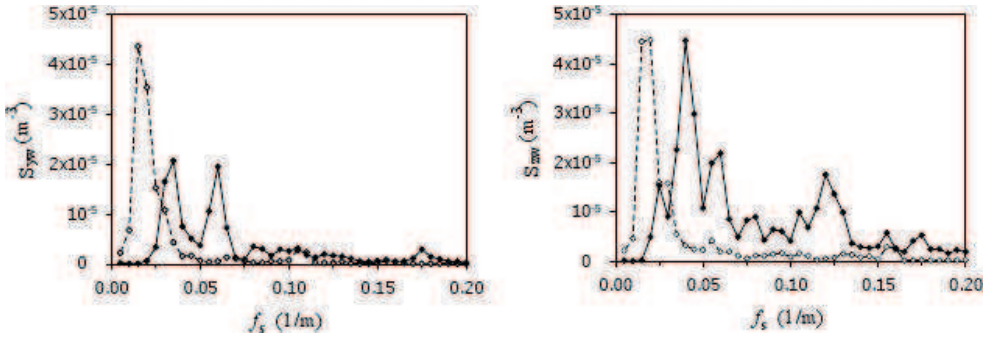

Fig. 3. Power spectral density of lateral (left panel) and vertical (right panel) track irregularities for two track sections: I (dashed line) and II (solid line) of different track quality: QN1, QN2; the PSD is a function of spatial frequency f_s

The rms body accelerations are calculated at the body centre-of-mass (COM) and at four other positions on the longitudinal principal axis (LPA) of the car body: two of these points are located above the rear and front bogies and two other points are at the intermediate locations, 5 m from the COM. For track section I (with better track quality) and velocities v up to 120 km/h, the rms *lateral* accelerations $a_{yb;\mathrm{rms}}(f)$ found at positions symmetric with respect to the COM are close to each other, especially for the frequency f corresponding to the maximum of $a_{yb;\mathrm{rms}}(f)$; see Fig. 4. For velocities v up to 160 km/h the maximum values of $a_{yb;\mathrm{rms}}(f)$ increase significantly when we move away from the body COM and they become a few times larger for most distant positions. However, with increasing velocity v the values of $a_{yb;\mathrm{rms}}(f)$ for various positions become relatively closer to each other so that the differences in ride comfort (related to lateral vibrations) experienced by passengers located at various parts of the car body are smaller. For the highest investigated velocity v = 200 km/h the maximum values of $a_{yb;\mathrm{rms}}(f)$ are largest in

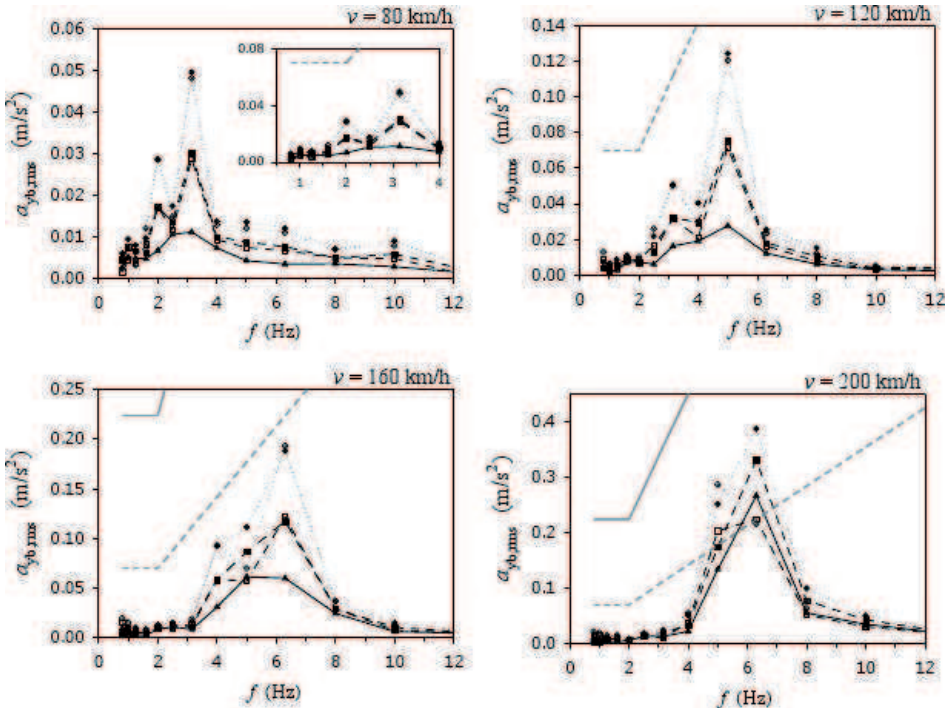

Fig. 4. Rms lateral body acceleration $a_{yb;\mathrm{rms}}(f)$ for track section I for various vehicle velocities v and positions x_b on the LPA of the car body: at the body COM $x_b = 0$ m (triangles), at the points $x_b = -8.75$ m (open circles) $x_b = 8.75$ m (circles) lying above rear and front bogies, respectively, and at intermediate locations $x_b = -5$ m (open squares), $x_b = 5$ m (squares). The grey lines mark the reduced comfort (dashed) and fatigue-decreased proficiency (solid) boundaries

the most front part of the car body and are smaller in the rear part than at the body COM.

For track section I, the rms lateral acceleration exceeds the comfort boundary only for $v = 200$ km/h – this occurs in the frequency range 5 Hz$\leq f \leq 7$ Hz for all investigated locations on the body LPA. The position $f_{\max}$ of the main maximum of $a_{yb;\mathrm{rms}}(f)$ changes with the vehicle velocity: from $f_{\max} = 3.15$ Hz for $v = 80$ km/h to $f_{\max} = 6.3$ Hz for $v = 200$ km/h For given v, the frequency $f_{\max}$ is usually the same for all positions, though there are some deviation from this rule: at the body COM for $v = 160$ km/h and at the point $x = -8.75$ m for $v = 200$ km/h; see Fig. 4.

Simulations done for track section II (with lower track quality) give the *lateral* rms body accelerations that have remarkably different behaviour than for section I, corresponding to better track condition; see Fig. 5. The largest values of $a_{yb;\mathrm{rms}}(f)$ now occur in the most front part of the car body. The smallest values – among rms accelerations at the five chosen locations – are obtained at the point $x = -5$ m in the rear body part. Such characteristic dependence of $a_{yb;\mathrm{rms}}(f)$ takes place – for all investigated velocities – for $f \geq 10$ Hz. For $f \geq 10$ Hz the dependence of the rms

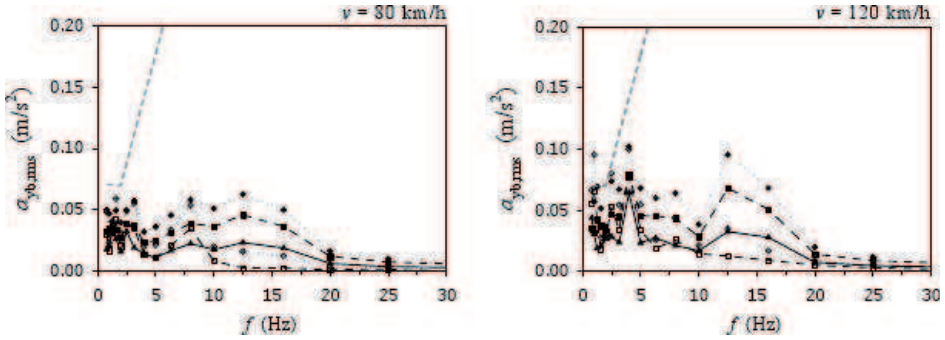

Fig. 5a. The rms lateral body acceleration $a_{yb;\mathrm{rms}}(f)$ for track section II for various positions x_b on the car body LPA and v = 80 km/h, 120 km/h; the lines are marked as in Fig. 4.
The frequency range 0.8-30 Hz

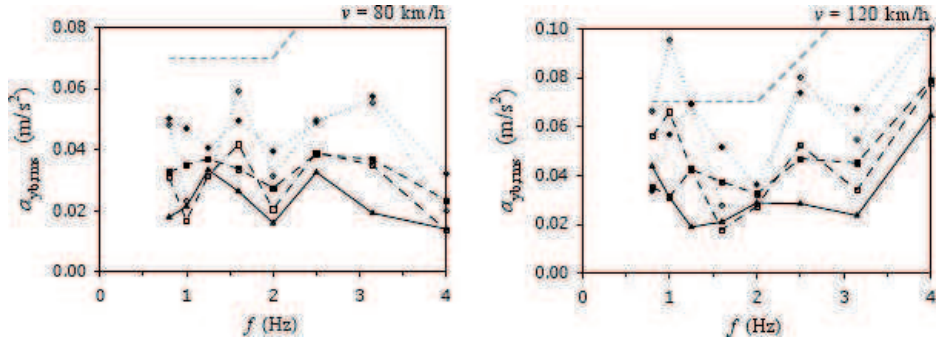

Fig. 5b. The rms lateral body acceleration $a_{yb;\mathrm{rms}}(f)$ for track section II for various positions x_b on the car body LPA and v = 80 km/h, 120 km/h; the lines are marked as in Fig. 4.
The frequency range 0.8-4 Hz

acceleration $a_{yb;\mathrm{rms}}(f)$ on the position within the car body is more complex. This is illustrated in Fig. 5 for v = 80 km/h and v = 120 km/h.

The rms *vertical* body accelerations obtained at different locations within the car body are closer to each other than in the case of the lateral accelerations. This is true for all considered velocities and both track sections. It is seen in Figs. 6 and 7 that – in the most of the relevent frequency range – the values of $a_{yb;\mathrm{rms}}(f)$ are largest at the positions in the most front part of the body and are smallest in its most rear part. This dependence of $a_{yb;\mathrm{rms}}(f)$ on the position reverses completely in a narrow interval of higher frequencies (around 10 Hz for v = 80 km/h or 20 Hz for v = 160 km/h) but it occurs only for track section I. The values of $a_{yb;\mathrm{rms}}(f)$ are larger for track section II (with lower track quality) than for section I and the comfort boundary is exceeded for v = 120 km/h at the most distant point in the front part of the car body.

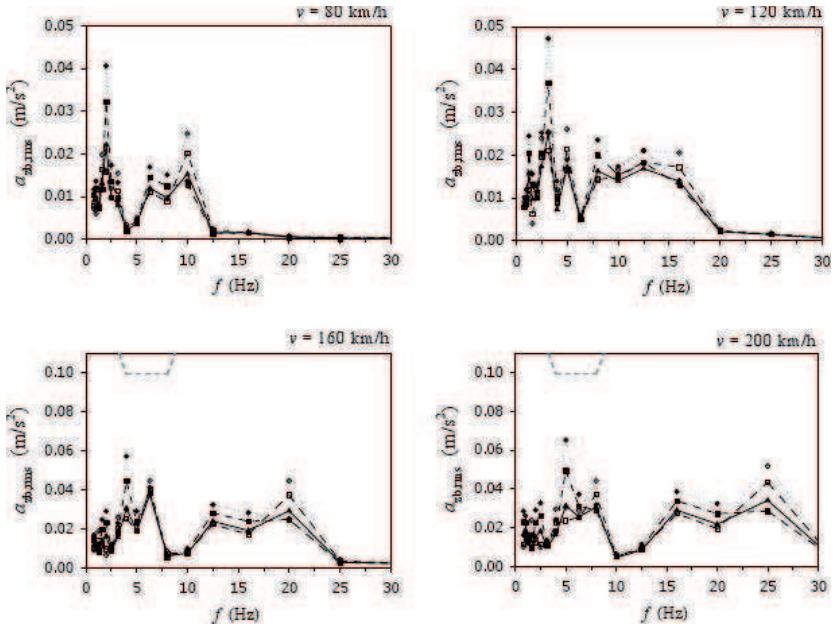

Fig. 6a. The rms vertical body acceleration $a_{yb;\mathrm{rms}}(f)$ for track section I for various vehicle velocities v and positions on the body LPA; the lines are marked as in Fig. 4.

The frequency range 0.8-30 Hz

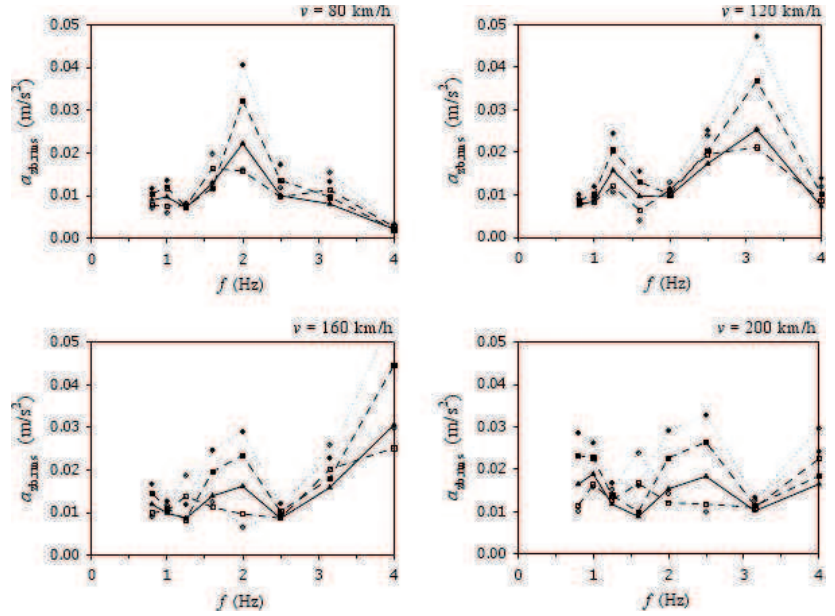

Fig. 6b. The rms vertical body acceleration $a_{yb;\mathrm{rms}}(f)$ for track section I for various vehicle velocities v and positions on the body LPA; the lines are marked as in Fig. 4.

The frequency range 0.8-4 Hz

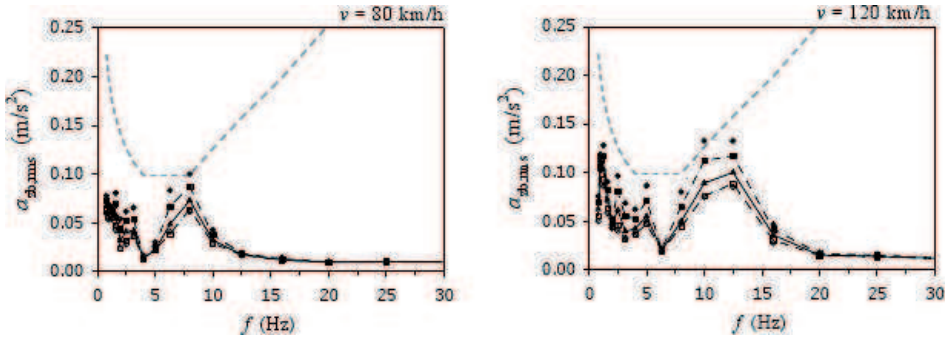

Fig. 7a. The rms vertical body acceleration $a_{yb;\mathrm{rms}}(f)$ for track section II for various positions x_b on the car body LPA and v= 80 km/h; the lines are marked as in Fig. 4.
The frequency range 0.8-30 Hz.

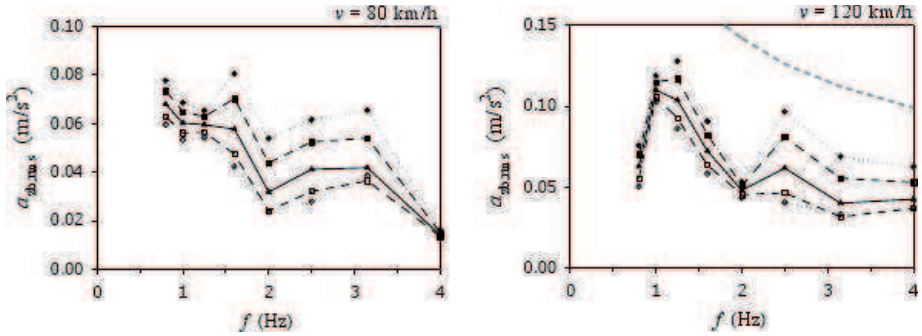

Fig. 7b. The rms vertical body acceleration $a_{yb;\mathrm{rms}}(f)$ for track section II for various positions x_b on the car body LPA and v= 80 km/h, 120 km/h; the lines are marked as in Fig. 4.
The frequency range 0.8-4 Hz

3. Ride comfort – frequency weighting method

3.1. Calculation method

A synthetic index of ride comfort can be obtained from the rms accelerations in 1/3 octave ban ds $(f_k - \Delta f_k/2, f_k + \Delta f_k/2)$ by using suitable frequency-dependent weighting functions $w_\eta(f_k)\,(\eta = y, z)$. According to the ISO 2631-1 and PN 91/S-04100 standards [4,11], the weight functions $w_\eta(f_k)$ are equal to 1 for frequency bands for which the reduced comfort and fatigue-decreased proficiency boundaries for the rms accelerations are lowest and they are smaller than 1 for other bands: $w_\eta(f_k) < 1$; see Fig. 8. Then, the frequency-weighted acceleration is defined as

$$a_{\eta b;w} = \left(\int_{f_{\min}}^{f_{\max}} S_{\eta b}(f)\, w_\eta^2(f)\, df \right)^{1/2} = \left(\sum_k a_{\eta b;rms}^2(f_k)\, w_\eta^2(f_k) \right)^{1/2} \quad (\eta = y, z) \qquad (4)$$

and the ride comfort is evaluated by comparing $a_{\eta b;w}$ with appropriate boundary values given in the ISO 2631-1 and PN 91/S-04100 standards [4,11].

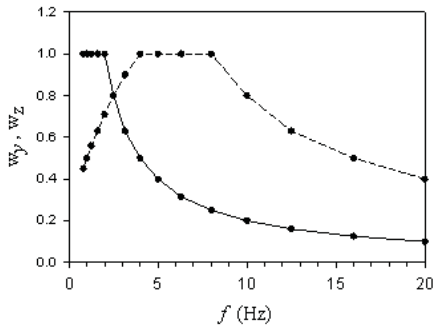

Fig. 8. The weight functions $w_y(f)$ (solid line), $w_z(f)$ (dashed line) used for calculation of weighted rms lateral and vertical body acceleration $a_{yb;w}$ and $a_{zb;w}$ with Eq. (4), according to [4,11]

3.2. Results – weighted rms accelerations

The weighted lateral and vertical rms body accelerations $a_{yb;w}, a_{zb;w}$ obtained for track sections I and II are shown in Fig. 9. It is clearly seen for both directions the weighted acceleration is much larger for track section II – over three times in the case of $a_{zb;w}$. However, both accelerations $a_{yb;w}, a_{zb;w}$ are below the comfort boundary for both track sections and all vehicle velocities (apart for $a_{yb;w}$ for v = 200 km/h on track section II).

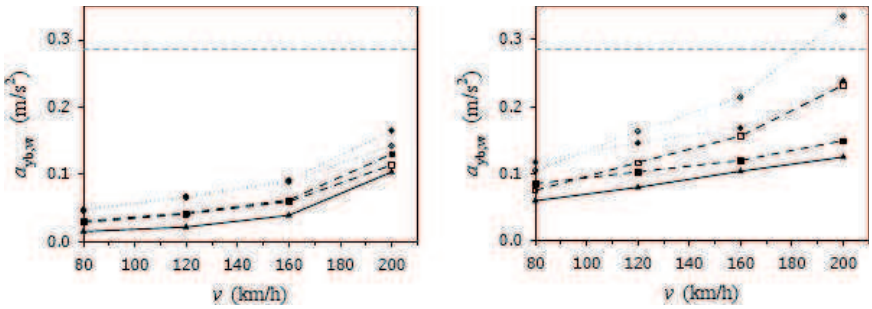

Fig. 9. The weighted rms lateral body accelerations $a_{yb;w}$ for track section I (left panel) and section II (right panel) and various positions x_b on the car body LPA (marked with the same symbols as in Fig. 4). The grey line dashed line marks the reduced comfort boundary

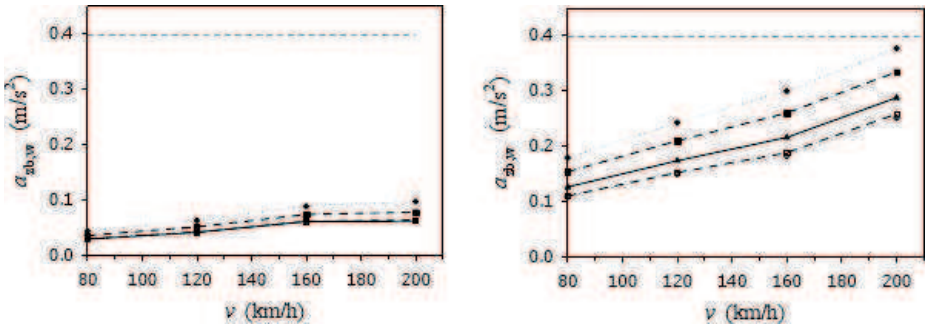

Fig. 10. The weighted rms vertical body accelerations $a_{zb;w}$ for track section I (left panel) and II (right panel) and various positions x_b on the car body LPA (marked with the same symbols as in Fig. 4). The grey line dashed line marks the reduced comfort boundary

It should be stressed that the results obtained in simulation on track section II for v = 160, 200 km/h are given here only for comparison with the results found for section I since these two velocities exceed the maximum speed limit for on a track of QN2 quality.

4. Conclusions

The performed simulations show that it is very important to include the effect of track quality in evaluation of the ride comfort. This effect is found to be particularly strong for the vertical body acceleration. The ride comfort also depends strongly on the vehicle velocity and passenger's position. These conclusions are confirmed by both methods used for comfort evaluation in the present work. The spectral analysis that gives the rms accelerations is a more accurate since it allows for detailed evaluation how vehicle vibrations affect passenger's ride comfort. This is related to variable effect of vibrations with various frequencies on individual parts of human body. The calculation of weighted rms body accelerations provides an easier way of comparing the ride comfort for various situations. However, this method of ride comfort evaluation is less accurate since there are cases for which the weighted rms acceleration satisfies the comfort criterium while the rms acceleration exceeds the comfort boundary for some specific frequencies; two such cases have presently been found for the lateral rms body acceleration; see Figs. 4, 5, 9.

The author wishes to acknowledge the financial support provided by the Ministry of Science and Higher Education (Project No N N509 4040360).

References

1. Da Silva G.: Measurements of comfort in vehicles, Measurement Science and Technology, vol. 13, pp. R41-R60, 2002.

2. Griffin M.J.: Handbook of Human Vibration, Academic Press, 1990.
3. Iwnicki S. (ed.): Handbook of Railway Vehicle Dynamics, CRC Press Inc., 2006.
4. ISO 2631-1: Mechanical Vibration and Shock. Evaluation of human exposure to whole-body vibration. Part 1: General Requirements, International Organization for Standardization, 1985 and 1997.
5. Kalker J.J.: A fast algorithm for the simplified theory of rolling contact, Vehicle System Dynamics, vol.11, 1-3, 1982.
6. Kardas-Cinal E.: Investigation of ride comfort in a railway vehicle in the presence of random track irregularities, Archives of Transport, vol. 18, issue 1, pp. 5-16,Warsaw 2006.
7. Kardas-Cinal E.: Analiza komfortu jazdy i bezpieczeństwa przed wykolejeniem pojazdu szynowego. Zeszyty Naukowe Instytutu Pojazdów Wydział SiMR Politechniki Warszawskiej, Mechanika Ekologia Bezpieczeństwo Nr 1 (60) 2006, Warszawa 2006, s. 121-130.
8. Kardas-Cinal E.: Running safety and ride comfort of a railway vehicle in the presence of random track irregularities, Proceedings of International Conference on Simulation Based Engineering and Sciences (TCN CAE 2008) 16-17.10. 2008, Venice, Italy.
9. Kardas-Cinal E.: Comparative study of running safety and ride comfort of railway vehicle, Prace Naukowe Transport z.71, pp 75-84. Oficyna Wydawnicza Politechniki Warszawskiej, Warszawa 2009.
10. Kim Y.-G., Kwon H.-B., Kim S.-W., Park C.-K. and Park T.-W.: Correlation of ride comfort evaluation methods for railway vehicles, Proc. Instn Mech. Engrs Part F: J. Rail and Rapid Transit, vol. 217, pp. 73-88, 2003.
11. Polska Norma PN-91/S-04100: Drgania. Metody badań i oceny drgań mechanicznych na stanowiskach pracy w pojazdach. Polski Komitet Normalizacji, Miar i Jakości, 1991.
12. Suzuki, H.: Research trends on riding comfort evaluation in Japan, Proc. Instn Mech. Engrs, Part F: J. Rail and Rapid Transit, vol. 212(F1), pp. 61-72, 1998.
13. Zboiński K.: Metodyka modelowania dynamiki pojazdów szynowych z uwzględnieniem zadanego ruchu unoszenia i jej zastosowania. Prace Naukowe Transport z. 43. Oficyna Wydawnicza Politechniki Warszawskiej, Warszawa 2000 (in Polish).
14. Zieliński: T.P. „Cyfrowe przetwarzanie sygnałów: od teorii do zastosowań", WKŁ 2005 (in Polish).